

Large Eddy Simulation of Hydrogen-Enriched Methane-Air Premixed Flames in a Confined Swirl Burner

David Cicoria, and C.K. Chan

Abstract—Large eddy simulation (LES) is employed to investigate the effects of hydrogen addition on lean CH₄-air turbulent confined swirling premixed flames for mixtures up to 50% of hydrogen in volume. The subfilter combustion term representing the interaction between turbulence and chemistry is modelled using the PaSR model, along with complex chemistry using a skeletal mechanism based on GRI-MECH3.0. At constant swirl number and equivalence ratio, results show a similar trend as in experiments concerning the flame shape and stabilization mechanism. Increasing hydrogen in the fuel mixture leads to an increase of turbulent flame speed, reactivity, flame temperature and NO emissions. Streamline profiles of mean velocity highlight the change in flame shape at higher hydrogen content due to a big jump in velocity inside the flame, and the structural modification of the outer recirculation zone. Independently of the equivalence ratio, the mean flame shape is shorter and turbulent flame thickness decreases as hydrogen is increased. Also, heat release becomes less sensitive to the change of equivalence ratio when hydrogen is more present in the fuel mixture.

Index Terms—Turbulent premixed combustion, large eddy simulation, hydrogen-enrichment of methane flames, swirl, finite rate chemistry, flame stability

I. INTRODUCTION

HYDROGEN-enrichment consists of a solution to enhance stability and reduce pollutant emissions of lean premixed flames. Hydrogen enrichment has been found to extend the lean flammability limit and to reduce CO, NO_x and UHC emissions in spark ignition engines [1], [2] and in gas turbines [3], [4]. Several studies have focused on fundamental aspects of swirling H₂-CH flames. It has been pointed out that hydrogen-enriched flames exhibit greater laminar flame speeds, increased resistance to strain and extended lean flammability limits [5], [6], [7]. With the increase of hydrogen in the fuel mixture, more NO_x emissions have been observed in the upstream region of the flame, whereas further downstream, similar levels have been reported for different mixtures at the same adiabatic flame temperature [6]. To further characterize the effects of swirl on flow dynamics with hydrogen-enrichment, Kim et al. [8], [9] carried out two studies of confined and non-confined premixed swirling

Manuscript received February 26, 2017; revised March 24, 2017. This work was partially supported by a studentship of The Hong Kong Polytechnic University and grants from the Research Committee of The Hong Kong Polytechnic University (Grant No G-UC26 and G-YBCL).

D. Cicoria is with the Department of Applied Mathematics, The Hong Kong Polytechnic University, Kowloon, Hong Kong, e-mails: david.cicoria@connect.polyu.hk, david.cicoria@gmail.com

C.K. Chan is with the Department of Applied Mathematics, The Hong Kong Polytechnic University, Kowloon, Hong Kong, e-mail: ck.chan@polyu.edu.hk

flames. They found out that higher combustibility of hydrogen enhances flame stability with hydrogen addition, both at low and high swirl strengths to the mixture. Hydrogen addition led to a shift of the reaction zone upstream of the flame, causing an increase in NO formation in this area due to higher peak temperatures of flame. However, their studies only considered hydrogen in the fuel mixture for up to 9% in volume. In this paper, different characteristics of the flame such as flame stability and pollutant emissions are studied by means of LES. Fuel mixtures of methane-hydrogen up to 50% of hydrogen in volume are considered to further examine the effects of hydrogen in a confined premixed swirl burner.

II. LES COMBUSTION MODELLING AND NUMERICAL PROCEDURE

In this paper, compressible Navier-Stokes equations with energy and species transport conservation equations are used with a low Mach number approach. The open source code OpenFOAM (Open Field Operation and Manipulation) [10], based on finite volume is used in this study. For the convective and diffusive terms, 2nd order accuracy is achieved in space using central difference scheme with linear interpolation, along with a normalized variable diagram (NVD) scheme. PISO algorithm is chosen to solve the unsteady Navier-Stokes equations using 3 pressure and momentum correctors (1 outer and 3 inner iterations) with residuals criterion of 10⁻⁹. Time integration is carried out using an implicit 2nd order quadratic backward approximation. The pressure equation is solved using a generalized geometric-algebraic multi-grid (GAMG) solver along with a Gauss-Seidel smoother. Concerning the velocity field and other scalar fields, the code uses a preconditioned bi-conjugate gradient (PBiCG) solver for skew-symmetric matrices with the diagonal incomplete LU (DILU) matrix used as preconditioner. The maximum CFL (Courant-Friedrichs-Lewy) number allowed in the simulations is 0.4. LES equations of reacting flows are obtained by both Favre and implicit filtering operations and are written as

$$\begin{cases} \frac{\partial \bar{\rho}}{\partial t} + \frac{\partial}{\partial x_i} (\bar{\rho} \tilde{u}_i) = 0 \\ \frac{\partial}{\partial t} (\bar{\rho} \tilde{u}_i) + \frac{\partial}{\partial x_j} (\bar{\rho} \tilde{u}_i \tilde{u}_j) = -\frac{\partial \bar{p}}{\partial x_i} + \frac{\partial}{\partial x_j} [\bar{\tau}_{ij}] - \bar{\rho} (\tilde{u}_i \tilde{u}_j - \tilde{u}_i \tilde{u}_j) \\ \frac{\partial}{\partial t} (\bar{\rho} \tilde{Y}_k) + \frac{\partial}{\partial x_i} (\bar{\rho} \tilde{u}_i \tilde{Y}_k) = -\frac{\partial}{\partial x_i} \left[\bar{V}_{k,i} \tilde{Y}_k + \bar{\rho} (\tilde{u}_i \tilde{Y}_k - \tilde{u}_i \tilde{Y}_k) \right] \\ \quad + \bar{\omega}_k \quad ; \quad k = 1, \dots, N, \\ \frac{\partial}{\partial t} (\bar{\rho} \tilde{h}^s) + \frac{\partial}{\partial x_i} (\bar{\rho} \tilde{u}_i \tilde{h}^s) = \frac{\partial}{\partial x_i} \left[\bar{\lambda} \frac{\partial \bar{T}}{\partial x_i} - \bar{\rho} (\tilde{u}_i \tilde{h}^s - \tilde{u}_i \tilde{h}^s) \right] \\ \quad - \sum_{k=1}^N h_k^o \bar{\omega}_k \quad ; \quad k = 1, \dots, N, \end{cases} \quad (1)$$

where usual symbols are used to describe the compressible Navier-Stokes equations. Thermophysical properties of the

species k are calculated using JANAF tables. The **unresolved Reynolds stress tensor** ($\widetilde{u_i u_j} - \widetilde{u_i} \widetilde{u_j}$) is modelled using the dynamic Smagorinsky model. The **unsolved species flux** ($u_i \widetilde{Y_k} - \widetilde{u_i} \widetilde{Y_k}$) and the **enthalpy flux** ($u_i \widetilde{h^s} - \widetilde{u_i} \widetilde{h^s}$) are described using a simple gradient assumption, giving ($u_i \widetilde{Y_k} - \widetilde{u_i} \widetilde{Y_k}$) = $-\frac{\nu_{sgs}}{Sc_t} \frac{\partial \widetilde{Y_k}}{\partial x_i}$ and ($u_i \widetilde{h^s} - \widetilde{u_i} \widetilde{h^s}$) = $-\frac{\nu_{sgs}}{Pr_t} \frac{\partial \widetilde{h^s}}{\partial x_i}$. The **filtered mass and heat diffusion fluxes** are also specified using a simple gradient hypothesis leading to $\overline{V_{k,i} Y_k} = -\overline{\rho} D_k \frac{\partial \widetilde{Y_k}}{\partial x_i}$ and $\overline{\lambda \frac{\partial T}{\partial x_i}} = \overline{\lambda} \frac{\partial \widetilde{T}}{\partial x_i}$. Concerning the diffusion coefficients D_k of the different species k , they are considered as constant for each of the species, obtained on a 1D laminar freely propagating flame using CANTERA [11]. They are defined considering the median values of Schmidt numbers Sc_k [12] such as $D_k = \nu / Sc_k$. Finally, the **filtered reaction rate** of species k , $\overline{\omega_k}$ is modelled using the finite rate chemistry Partially Stirred Reactor (PaSR) approach derived by Karlsson [13] along with the skeletal mechanism of Karalus [14] to handle CH₄-H₂ mixtures. For finite rate chemistry, integration of the source terms ω_k is realized by ISAT-CK7 [15], with a tolerance error of 1×10^{-4} in combination with the ‘‘SkeletalGRI’’ [14] mechanism. The numerical procedure used in this work has been previously validated by the authors [16] and Fooladgar et al. [17].

III. COMPUTATIONAL SETUP

The swirl burner used in this work is based on the reduced-scale model of Nogenmyr et al. [18]. Four tangential inlets and a radial swirler allow the burner to be operated from low to high swirl numbers. The main benefit of studying a reduced-scale combustor resides in the potential reproduction of this computational domain for CFD studies. Indeed, in implicit filtering of LES as used in this work, the filter is of the same size as the mesh. By using reduced models, it allows to mesh the computational domain with cell size of around that of laminar flame thickness and allowing the use of simpler combustion models. Fig. 1 shows a schematic representation of the burner.

By definition, the swirl number Sw is specified as the ratio of the axial flux of angular momentum to the product of the axial flux of axial momentum with a characteristic radius R . For a tangential jet-induced swirl flow, it can be assessed as

$$Sw = \frac{\int_0^R U_x U_{\theta} r^2 dr}{R \int_0^R U_x^2 r dr} \approx \frac{\pi D}{16WH} \frac{D - W}{(\dot{m}_x / \dot{m}_r + 1)^2} \quad , \quad (2)$$

where D is the diameter of the axial inlet, W and H are respectively the width and height of the tangential jets and \dot{m}_x / \dot{m}_r is the ratio of the axial to the tangential mass flow rates. An overall Reynolds number Re is then defined as

$$Re = \frac{\dot{m}_x + \dot{m}_r}{\mu(\pi D/4)} \quad , \quad (3)$$

where μ is the dynamic viscosity of the unburned mixture. Flames with a global equivalence ratio ϕ are investigated for different mixtures composed of methane-hydrogen-air with the volume fraction β of hydrogen in the CH₄-H₂ blend defined by $\beta = X_{H_2} / (X_{H_2} + X_{CH_4})$.

In the following section, the computational setup is first presented for the LES simulations with the specification of the different boundary conditions. Comparison of the results obtained in the simulations with experiments is only visual.

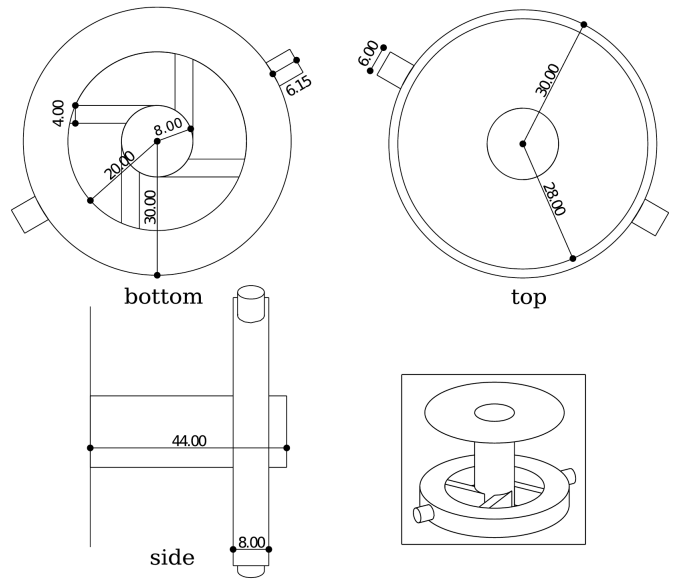


Fig. 1: A schematic drawing of the burner. All units are in millimeter.

Concerning the prediction of species NO, the results are in the same range as what has been measured by Fooladgar [19] and they are only studied numerically. A range of flow and flame configurations have been simulated by Cicoria [20], and configurations of simulations in this paper are given in Table I.

TABLE I: Parameters for the different configurations of study.

Sw	ϕ	β (%)	Re
0.7	0.85	0	6000
0.7	0.85	10	6000
0.7	0.85	20	6000
0.7	0.85	30	6000
0.7	0.85	40	6000
0.7	0.85	50	6000
0.7	0.95	0	6000
0.7	0.95	20	6000
0.7	0.95	40	6000

Fig. 2 shows an overview of the computational domain with the location of the flame in a premixed case, represented by the instantaneous fuel mass fraction at 0.01. The numerical domain is composed of the swirler, combustion chamber and a large rectangular region downstream of the combustor exit to consider the presence of air atmosphere and to diminish the impact of outflow boundary conditions in the combustion chamber. Dimensions of the computational configuration are given in Fig. 1.

The computational mesh consists of 2.5 million hexahedral cells, which are body fitted inside the domain. Inside the burner and combustor, the resolution is around $\Delta_x = 0.5$ mm per cell, leading to 34 cells over the diameter of the axial inlet and to maximum ratio of filter size to thermal flame thickness of 2 for the different reacting flows. For all wall boundary conditions, a boundary layer constituted of

4 layers with a growth rate of 1.2 is created to ensure the criteria of application of the different wall models used for these area.

Fully developed turbulent velocity profiles, calculated based on Re and swirl number of each case, and uniform species mass fractions, defined based on the global equivalence ratio ϕ , are specified at all inlet boundaries. At the walls, a no-slip boundary condition is specified for velocity with zero gradients for all scalars. The temperature of the wall in reacting cases is defined by an assessed profile, based on experimental results of Nogenmyr et al. [18]. To avoid the creation of numerical waves when physical waves (such as acoustic ones) reach the atmospheric outlet boundary, a partially reflective outlet boundary proposed by Rudy and Strickwerda [21] is imposed for pressure, and also ensuring flux conservation for the velocity.

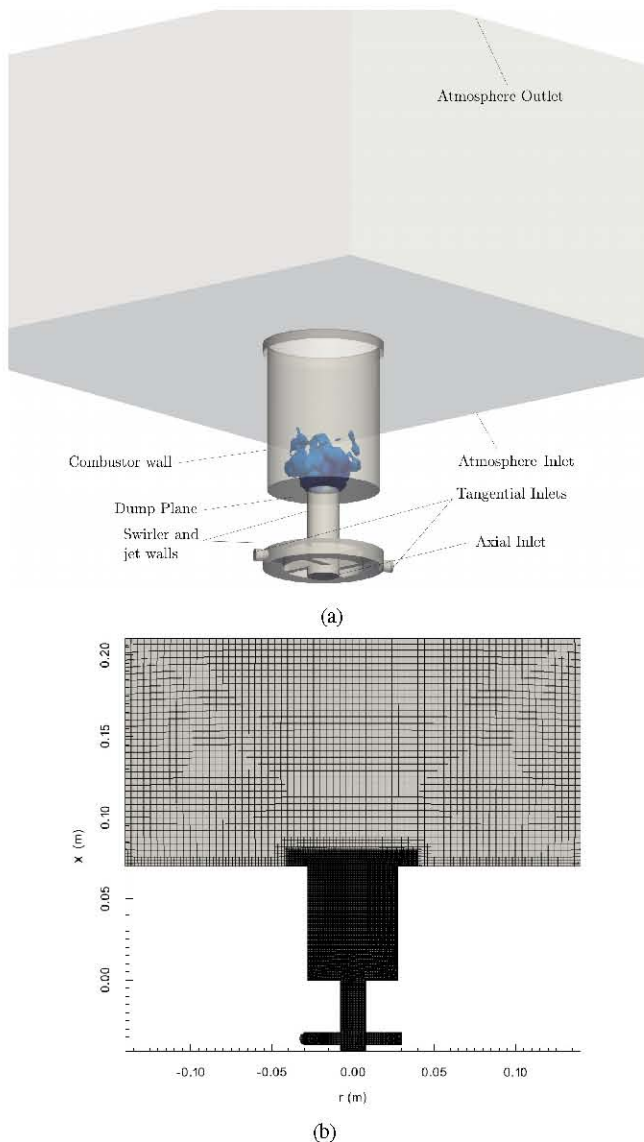


Fig. 2: An overview of (a) computational domain and (b) grid distribution in the whole domain (Cicoria [20]).

IV. RESULTS AND DISCUSSION

A. Comparison at Constant Equivalence Ratio and Swirl Number

Different swirling flames are first investigated considering a fixed swirl number of 0.7 and equivalence ratio $\phi = 0.85$. Four different mixtures of methane-hydrogen with $\beta = 0, 0.1, 0.3$ and 0.5 are then studied at these conditions. All simulations have been run to 0.1 s to ensure statistical convergence of the flow. Fig. 3 shows a comparison between long exposure quantized pictures taken during the experiments and the flame shape from the numerical simulations for the case of $Re = 5000$, $\phi = 0.85$ and $Sw = 0.7$. For the computational cases, flame shape is represented by the mean mass fraction of the intermediate species OH, which is usually considered in experiments with PLIF. The comparison between experiments and simulations is only qualitative. It can be seen in both results that flame stability is strengthened when injecting more hydrogen in the unburned mixture. This is confirmed by the evolution of flame shape and also by the blue color which becomes more prominent at higher β , indicating higher flame temperature from the experiments and higher concentration of intermediate species OH from the numerical simulations. For the flame shape, they differ between experiments and simulations. However, the trend in the evolution by steadily increasing β is the same, showing the potential of our LES simulations.

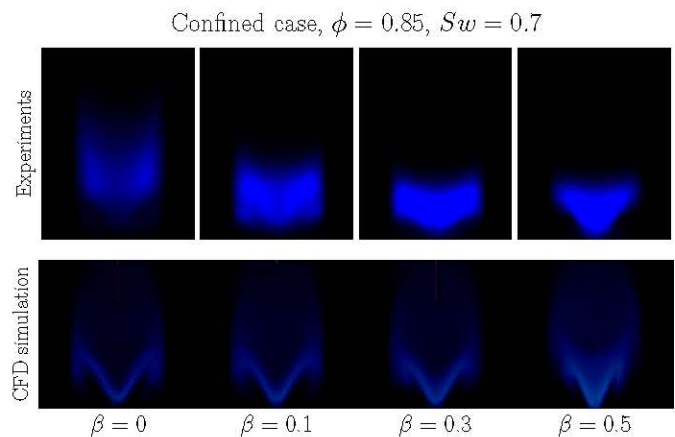


Fig. 3: Comparison between quantized experimental pictures and representation of mean OH mass fraction in numerical simulations.

Fig. 4 shows the planar cuts of mean distribution of CO and NO for all cases at $\phi = 0.85$ and $Sw = 0.7$. From the evolution of CO distribution with increasing hydrogen, the same features as in Fig. 3 are seen. Indeed, the shape of CO distribution follows the same trend as in the pictures, not only in the shape but also in the spread of the CO species. Precisely, for pure methane the spread is more important and then decreases with the increase in hydrogen. This is due to the increase in flame stability, as higher amounts of CO are found in a smaller defined region. Fig. 4 also shows the distribution of pollutant NO, which is highly related to the temperature and shape of the flame. At constant equivalence ratio, increasing β results in an increase of NO emission. From the previous measurements of Fooladgar [19], NO

formation only amounts to several ppm as in the simulations. Another interesting point is the location of main formation of NO, which is mainly related to the flame shape and stabilization. Considering the x direction as axial direction of the flow, it can be seen that by increasing hydrogen fraction β , the main formation of NO occurs at higher values of x. The bottom of the central recirculation zone (CRZ), where NO is usually formed in higher amount due to the low velocity, and the longer time for the different reactions, is gradually higher in the combustor with β .

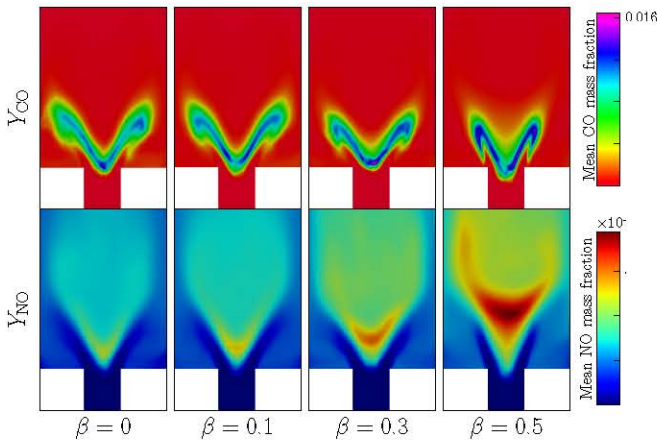


Fig. 4: Planar cuts of the mean distribution of CO and NO for all cases at $\phi = 0.85$ and $Sw = 0.7$.

Fig. 5 compares radial profiles of mean mass fraction of NO (ppm) and mean temperature for all configurations at $\phi = 0.85$ and $Sw = 0.7$ and different axial positions, when β is increased from 0 to 0.5. The magenta dotted lines specify a mean temperature in the combustor of 1800 K, above which thermal NO production is usually more prominent. Results in Fig. 5 confirm the above discussion of Fig. 4 concern the formation of NO as for any axial position x, the mass fraction of NO is more important when β is higher. For different cases and starting from $x = 0$ mm, NO formation occurs mostly in the centre of the configuration at $r = 0$ mm and decreases with the increase in r . By moving upward in x, similar behaviour is seen up to $x = 20$ mm, but also with progressively increase of the formation of NO in the centre. Indeed, for $x > 20$ mm, the behaviour changes as emissions are also present in the side, due to the fact that the CRZ has been reached at this height for all cases except for $\beta = 0$. For the case of $\beta = 0.6$, the CRZ has not been reached; the change in profile occurs at higher axial position. For $x > 30$ mm, the profiles of NO mass fraction are more steady with a decrease close to the walls. The position of $x \approx 30$ mm corresponds to where the experimental measurements have been realized. The results obtained here show the same trend of the measurements of Fooladgar [19]. The profiles of temperature also evolve in a similar way for each case with a progressive increase of temperature at fixed radial direction r when moving upwards along the axial axis.

Fig. 6 compares radial profiles of mean velocity magnitude U and mean rms fluctuation U_{rms} for all configurations at $\phi = 0.85$ and $Sw = 0.7$ at different axial positions when β is increased from 0 to 0.5. The jump in velocity is more

important when β is higher, highlighting the increase in turbulent flame speed with the increase of hydrogen. The different profiles evolve similarly for all mixtures except for $\beta = 0.5$. Indeed, for this mixture the flame angle is more acute and velocity stays higher in the centre of the geometry for higher axial direction till the CRZ is reached in comparison with the other cases. Concerning the mean rms fluctuations U_{rms} , they are at the same levels as reported previously by Fooladgar [19] and varying from 1 to 2 m/s along the radial direction r , and in correlation with the temperature profiles shown in Fig. 5.

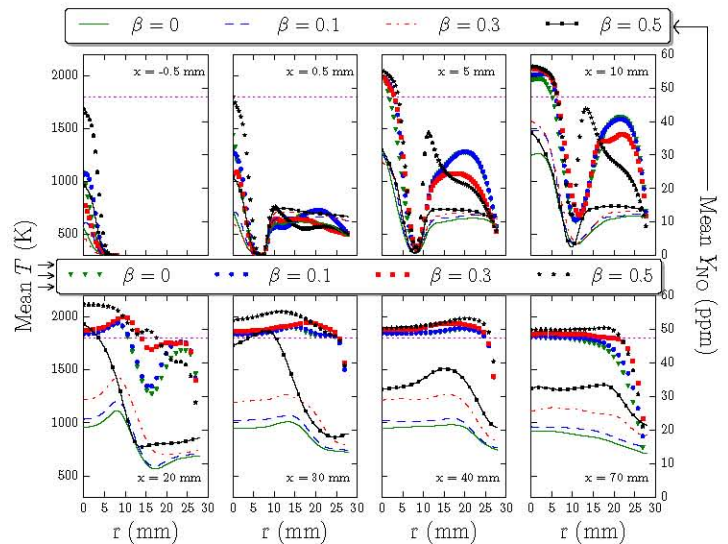


Fig. 5: Radial profiles of mean mole fraction of NO (lines) and mean temperature (markers) for all configurations at $\phi = 0.85$ and $Sw = 0.7$ at different axial positions and mixtures. Dotted lines in magenta indicate mean $T = 1800$ K.

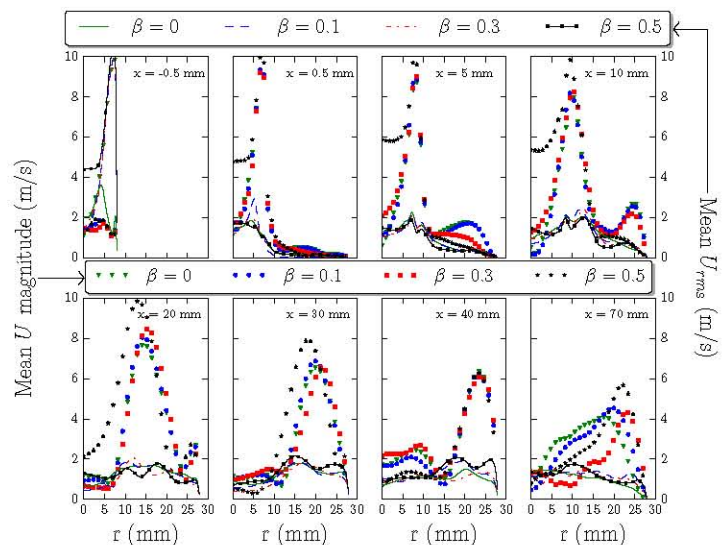


Fig. 6: Radial profiles of mean velocity magnitude U (markers) and mean rms fluctuation U_{rms} (lines) for all configurations at $\phi = 0.85$ and $Sw = 0.7$ at different axial positions and mixtures.

B. Variation of Equivalence Ratio

In this section, the swirl number is still fixed to $Sw = 0.7$ but two different equivalence ratios of 0.95 and 0.85 are studied for 3 mixtures of methane-hydrogen with $\beta = 0, 0.2$ and 0.4.

Fig. 7 shows the instantaneous iso-volumes of progress variable from 0.2 to 0.8 for the different cases, colored by the temperature profiles. One advantage of studying combustion with CFD simulations is the ability to represent the flame in three dimensions, when in experiments only 2D images can be obtained. It can be seen that at fixed equivalence ratio, flame gets shorter as hydrogen increases. The flame shape evolves similarly for both equivalence ratio against β , suggesting that hydrogen addition in both cases alter progressively the structure of the flame and modify its mechanism of stabilization as seen in Fig. 3. Indeed, for the cases of $\beta = 0.4$, the V-shape is more pronounced.

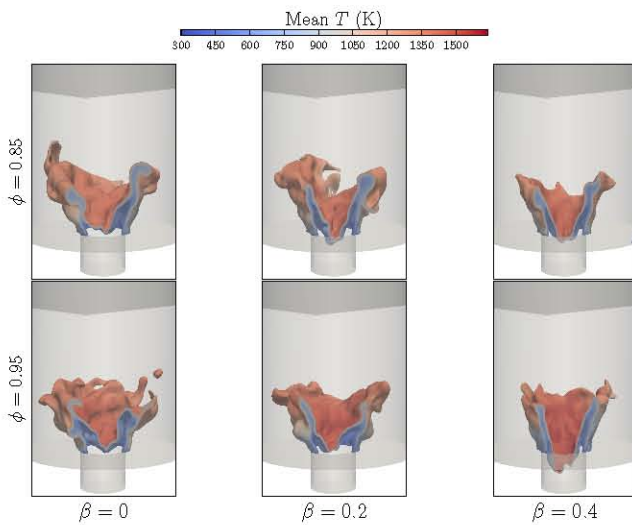


Fig. 7: Iso-volumes of progress variable over 0.2 - 0.8. One quarter of each volume is blanked to depict the temperature distribution inside the flame.

Fig. 8 shows the contours of mean velocity magnitude and surface streamlines as well as the values of iso-progress variable $c = 0.2, 0.5$ and 0.8 . It can be seen for all cases at $\beta = 0$ and 0.2 that the mechanism of stabilization of the flame is the same with the presence of a big central recirculation zone (CRZ) above the flame due to vortex breakdown and shear layers, and 2 corner or outer recirculation zones (ORZ) created due to sudden expansion of the flow when entering the combustion chamber. For these cases, the ORZ consists of one big vortex and a smaller one at the junction of the walls. With the change in fuel mixture to $\beta = 0.4$, and as flame speed increases and feeding velocity is adjusted to keep the same mass flow rates, flame shape changes as the jump in velocity is much higher in these cases. The shape of the ORZ is modified as the small vortex tends to expand and move the flame upwards, thus displaying a more acute V-shape. For any equivalence ratio, it can be seen that as hydrogen increases the CRZ location moves downstream as axial velocity is higher. From the iso-progress variable profiles, it can be seen that the mean flame shape is

shorter and turbulent flame thickness decreases as hydrogen increases for both equivalence ratios.

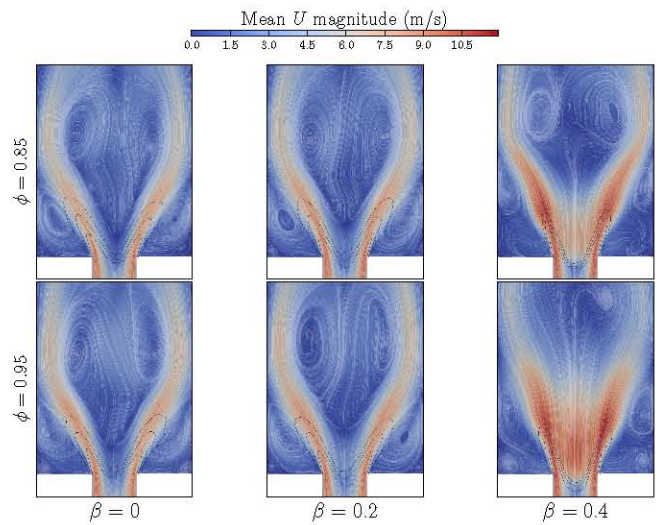


Fig. 8: Two dimensional profiles of mean velocity magnitude U for different cases. Streamlines of mean velocity are also represented in white for each case and the black lines denote the values of iso-progress variable of 0.2, 0.5 and 0.8.

Fig. 9 shows the contours of mean heat release and mean temperature for the different cases considered. Surface streamlines of mean velocity are also plotted over the background of the mean temperature field. The total heat release dQ is defined as the product of the source terms from the energy equation times the mesh cell volume,

$$dQ = \Delta_x^3 \sum_{k=1}^N (h_k^o \bar{\omega}_k) = \Delta_x^3 \sum_{k=1}^N (h_k^o \kappa \bar{\omega}_k), \quad (4)$$

with the corresponding units of $J/s = kg \ m^2/s^3$.

The mean adiabatic flame temperature increases with equivalence ratio and also as hydrogen increases in the fuel mixture. For the cases of $\beta = 0.4$, due to the higher jump in velocity on the centerline, the area of highest temperature is bigger than for the other cases. For the heat release it is also expected to increase with the equivalence ratio and the fraction β . However, even though it is true for the case of pure methane ($\beta = 0$) that heat release decreases with equivalence ratio, it can be seen that as hydrogen content increases, there is lesser difference between each equivalence ratio. Indeed, for the highest level of hydrogen of $\beta = 0.4$, global heat releases are at the same levels. This is explained by the fact that the heat of methane's combustion in $kJ/kmol$ is 3 times higher than that of hydrogen. As more hydrogen replaces methane by volume, the gap between the mixtures of the same hydrogen-methane ratio β with different ϕ decreases.

Finally Fig. 10 shows the distribution of both mean mass fraction of NO and mean temperature. It can be seen for these equivalence ratios that the formation of NO is mainly a function of temperature as the temperature is higher in any case at $\phi = 0.95$ in comparison with the cases at $\phi = 0.85$. Concerning the location of the peak of Y_{NO} , they are located close to the central recirculation zone as seen previously in

Fig. 4. Indeed, NO formation is also a function of time and from a kinetic point of view is not always fast.

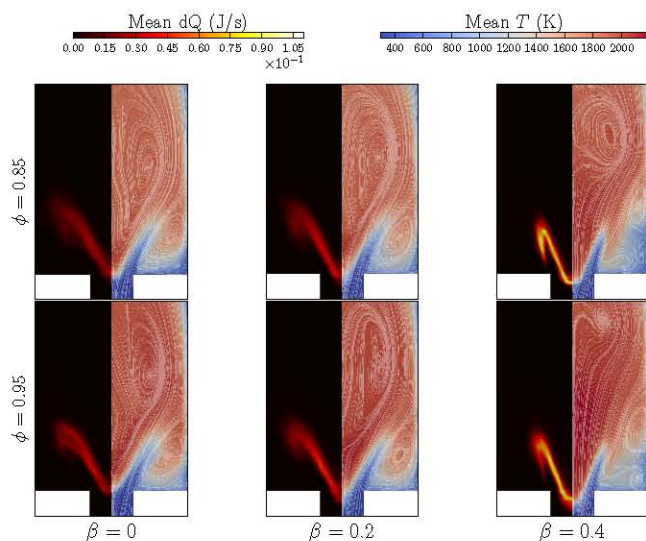


Fig. 9: Distribution of mean heat release (left) and mean temperature (right) for the different cases. Surface streamlines of mean velocity are also represented on background of the temperature field.

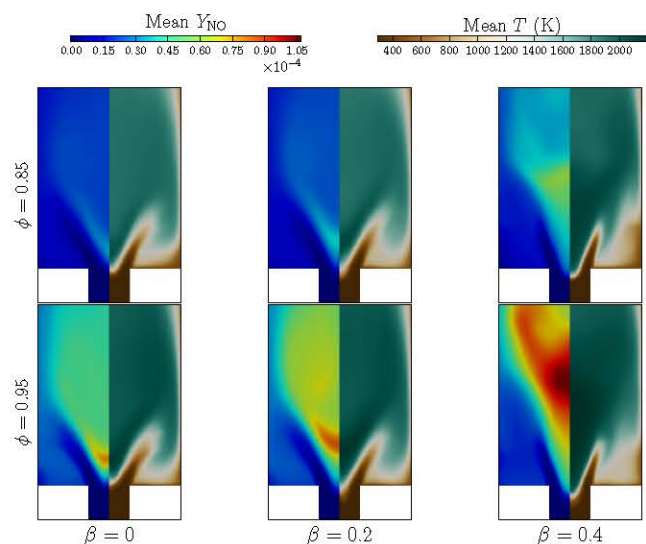


Fig. 10: Distribution of mean mass fraction of NO (left) and mean temperature (right) for the different cases.

V. CONCLUSION

A swirl burner has been investigated numerically using LES. Experiments have been conducted for visualization of the flame. The OpenFOAM CFD library has been used to simulate the flow dynamics. Interaction between chemistry and turbulence has been handled using LES with PaSR model, and chemical kinetics being described by the “SkeletalGRI” mechanism to represent the CH₄-H₂ premixed flames. LES have been run to explore the effects of hydrogen addition on this particular configuration. At constant swirl number and equivalence ratio, results show a similar trend as in experiments concerning flame shapes and stabilization mechanism. Increasing hydrogen in the fuel mixture leads to an increase of turbulent flame speed,

reactivity, flame temperature and NO emissions. Streamline profiles of mean velocity highlight the change in flame shape at higher fraction β due to a big jump in velocity inside the flame, and modifying the structure of the outer recirculation zone. Independently of the equivalence ratio, the mean flame shape is shorter and turbulent flame thickness decreases as hydrogen increases. Also, heat release is less sensitive to the change of equivalence ratio when hydrogen content increases in the fuel mixture.

REFERENCES

- [1] S. R. Bell and M. Gupta, “Extension of the lean operating limit for natural gas fueling of spark ignited engine using hydrogen blending,” *Combust. Sci. Technol.*, vol. 123, pp. 23–48, 1997.
- [2] C. G. Bauer and T. Forest, “Effect of hydrogen addition on the performance of methane-fueled vehicles. Part I: effect on SI engine performance,” *Int. J. Hydrogen Energy*, vol. 26, pp. 71–77, 2001.
- [3] D. N. Anderson, “Effect of hydrogen injection on stability and emissions of an experimental premixed prevaporized propane burner,” *NASA Tech. Memorandum TM X-3301*, 1975.
- [4] R. M. Clayton, “Hydrogen enrichment for low-emission jet combustion,” *Adv. Chem. Ser.*, vol. 166, pp. 267–286, 1978.
- [5] R. W. Schefer, D. M. Wicksall, and A. K. Agrawal, “Combustion of hydrogen-enriched methane in a lean premixed swirl-stabilized burner,” *Proc. Comb. Inst.*, vol. 29, pp. 843–851, 2002.
- [6] R. W. Schefer, “Hydrogen enrichment for improved lean flame stability,” *Int. J. Hydrogen Energy*, vol. 28, pp. 1131–1141, 2003.
- [7] G. S. Jackson, R. Sail, J. M. Plaia, C. M. Boggs, and K. T. Kiger, “Influence of H₂ on the response of lean premixed CH₄ flames to high strained flows,” *Combust. Flame*, vol. 132, pp. 503–511, 2003.
- [8] H. S. Kim, V. K. Arghode, M. B. Linck, and A. K. Gupta, “Hydrogen addition effects in a confined swirl-stabilized methane-air flame,” *Int. J. Hydrogen Energy*, vol. 34, pp. 1054–1062, 2009.
- [9] H. S. Kim, V. K. Arghode, and A. K. Gupta, “Flame characteristics of hydrogen-enriched methane-air premixed swirling flames,” *Int. J. Hydrogen Energy*, vol. 34, pp. 1063–1073, 2009.
- [10] H. G. Weller, G. Tabor, H. Jasak, and C. Fureby, “A tensorial approach to computational continuum mechanics using object-oriented techniques,” *Comput. Phys.*, vol. 12(6), pp. 620–631, 1998.
- [11] D. G. Goodwin, “Cantera: An open-source, extensible software suite for CVD process simulation,” in *Proceedings of CVD XVI and EuroCVD Fourteen*, M. Allendorf, F. Maury, and F. Teyssandier, Eds. The Electrochemical Society, 2003, pp. 155–162.
- [12] E. Giacomazzi, F. R. Picchia, and N. Arcidiacono, “A review of chemical diffusion: Criticism and limits of simplified methods for diffusion coefficient calculation,” *Comb. Theory Model.*, vol. 12, pp. 135–158, 2008.
- [13] J. A. Karlsson, “Modelling auto-ignition, flame propagation and combustion in non-stationary turbulent sprays,” Ph.D. dissertation, Chalmers University of Technology, Göteborg, 1995.
- [14] M. Karalus, “An investigation of lean blowout of gaseous fuel alternatives to natural gas,” Ph.D. dissertation, University of Washington, 2013.
- [15] S. B. Pope, V. Hiremath, S. R. Lantz, Z. Ren, and L. Lu, “ISAT-CK7: A Fortran 90 library to accelerate the implementation of combustion chemistry,” 2012. [Online]. Available: <http://tcg.mae.cornell.edu/ISATCK7>
- [16] D. Cicoria and C. K. Chan, “Large eddy simulation of lean turbulent hydrogen-enriched methane-air premixed flames at high karlovitz numbers,” *Int. J. Hydrogen Energy*, vol. 41(47), pp. 22479–22496, 2016.
- [17] E. Fooladgar, C. K. Chan, and K. J. Nogenmyr, “An accelerated computation of combustion with finite-rate chemistry using LES and an open source library for In-Situ-Adaptive Tabulation,” *Comput. Fluids*, vol. 146, pp. 42–50, 2017.
- [18] K. J. Nogenmyr, H. Cao, C. K. Chan, and R. K. Cheng, “Effects of confinement on premixed turbulent swirling flame using large eddy simulation,” *Comb. Theory Model.*, vol. 17(6), pp. 1003–1019, 2013.
- [19] E. Fooladgar, “Large Eddy Simulation and Experimental Analysis of a Swirl-Stabilized Flame under Preheated and/or Stratified Conditions,” Ph.D. dissertation, The Hong Kong Polytechnic University, 2016.
- [20] D. Cicoria, “Characterization of Turbulent Premixed Hydrogen-enriched Methane-Air Flames Using Large Eddy Simulation,” Ph.D. dissertation, The Hong Kong Polytechnic University, 2017.
- [21] D. H. Rudy and J. C. Strikwerda, “Boundary conditions for subsonic compressible Navier-Stokes calculations,” *Comput. Fluids*, vol. 9(3), pp. 327–338, 1981.